International Journal for Housing Science and Its Applications
Publish August 3, 2025. Volume 46, Issue 3 Pages 793-804

https://doi.org/10.70517/ijhsa46359

Computational analysis of kinetic modeling and micromechanism of fluoride ion adsorption process on metal composite surfaces

Tao Yu[1,*]
[1] School of Environment and Ecology, Hunan Agricultural University, Changsha, Hunan, 410011, China
Corresponding authors: (e-mail: ytjiayou123@163.com).

Abstract Fluoride contamination in water bodies is one of the serious environmental problems, and groundwater fluoride contamination is a constraint affecting the use of groundwater and even a threat to human health. Therefore, it is necessary to find widely applied and cost-effective methods for fluoride removal from water bodies. In this paper, we express the adsorption kinetics by constructing the reaction rate equation of the adsorption process and investigate the adsorption mechanism in the adsorption process by quasi-primary and quasi-secondary kinetic models. Langmuir isothermal and Freundlich isothermal models were set up sequentially to design the intermittent adsorption test. X-ray diffraction analysis and Fourier transform-infrared spectroscopy were used to calculate the kinetic and microscopic mechanisms of fluoride ions on the surface of metal composites. The fit R^2 of the proposed secondary kinetics at reagent concentrations of 10 mg/L, 30 mg/L and 100 mg/L were all 0.9999, and the fit of the proposed secondary kinetics model was much higher than that of the proposed primary kinetics model. A new peak was observed at 702.4553 eV for activated alumina (GAA) C, indicating the successful loading of fluoride species onto the GAA adsorbent.

Index Terms Adsorption process reaction rate, Adsorption kinetic model, Langmuir isotherm, Fourier transform, Microscopic mechanism

I. Introduction

Fluorine (F) is classified by the World Health Organization as one of the contaminants of human drinking water, and excessive intake can cause serious health hazards [1], [2]. The effects on human health may be beneficial if the concentration of F ions is between 0.5 and 1.5 mg/L, which will affect the incidence of dental caries [3]. On the contrary, excessive intake of F ions can lead to various diseases such as osteoporosis, arthritis, cancer and thyroid disorders [4], [5]. In view of the toxic effects of F ions on human health, there is an urgent need to find an effective method to remove excess F ions from drinking water.

In recent years, the main methods that have been reported for the treatment of F ions include precipitation, reverse osmosis, ion exchange and electrocoagulation [6], [7]. These methods are suitable for removing F ions from higher concentrations of industrial wastewater, while the main disadvantages for lower concentrations of F ions in drinking water are high maintenance and operating costs, low removal capacity, adverse effects on water quality and complex treatment procedures. Adsorption is a common contamination treatment method and among several methods for treating plants in water, it is low cost, simple in design and operation, and suitable for the removal of low concentrations of F ions [8].

At present, the main reported adsorbents for F ion removal are carbon-based materials, chitosan and its modified materials, metallic materials, polymers and resins, metal-organic skeleton materials and metal composites, etc., each of which has its advantages and disadvantages [9]-[11]. Common carbon materials have high specific surface area as well as controllable pore structure, and common carbon-based adsorbents used for fluoride removal are categorized as activated carbon, biochar and bone charcoal, carbon nanotubes, graphene and graphite-based materials [12]. However, single carbon materials have low adsorption activity for fluorine due to their surface structure, and surface modification is usually required to improve the adsorption performance. Natural minerals are natural single substances or compounds formed under geological action with relatively fixed chemical compositions, and natural minerals have the advantages of large scale, low cost, and simple operation in pollution control [13].

Natural minerals that have been studied for F ion removal can be categorized as clays, zeolites, calcium based minerals, SiO2, etc [14]. Ben Amor et al [15] used two Tunisian clay minerals as low-cost F-ion adsorbents to

remove excess fluoride from drinking water. Natural minerals Yi, M et al [16] utilized prepared red clay based polymeric microspheres (RM@GMs) and their ability to remove F ions from wastewater was investigated, which showed high adsorption capacity, selectivity and dynamic separation properties. Although natural minerals have the advantage of low cost for removing F ions, conventional mineral materials have low adsorption capacity and usually require modification or activation as well.

Resin is characterized by high molecular weight, good stability, and three-dimensional carbon chain backbone structure, and is likewise a commonly used material for adsorption of F ions [17].Gao, Y et al [18] simulated the adsorptive removal of F ions from wastewater by using an anion-exchange resin (IRA67) material, which was found to adsorb perfluorinated compounds (PFCs) and perfluorooctane sulfonate (PFOS) at 4.2 mmol/g and 5.5 mmol/g. Alrowais, R et al [19] developed a novel adsorbent material (OFW) from olive fruit resin and modified by hydroxyl radical pretreatment and quaternization, which enabled the material to exhibit good adsorption properties for F ions. The single resin material can only show college adsorption performance for high F ion concentration, and for drinking water with low F ion concentration, it is still necessary to modify the adsorption capacity by combining it with other materials such as metals or organics.

Metallic materials are characterized by efficient adsorption properties, high affinity for fluorine, and abundant surface hydroxyl groups [20]. Among all metal compounds, rare metals are difficult to be applied due to their high price, while cheap metal materials such as MgO, Fe2O3, and Al2O3 are more suitable for the preparation of fluoride removal materials [21]. Zhou, Q et al [22] developed a MgO-based adsorbent derived from Mg-MOF-74, which possessed excellent fluoride removal capacity as well as reusability for water treatment. Yang, K et al [23] in their study prepared a hierarchical porous nanosheets (HP-AMONTs) using Al2O3 and MgO metalloids and achieved 65.80% removal of F ions in ZnSO4 solution by combining kinetic and Langmuir isothermal adsorption models. Guo, W et al [24] reported a new method to synthesize MgO nanoparticles, a metallic material with high surface area and porosity, which can effectively remove fluoride ions from water with a maximum adsorption capacity of 372.65 mg/g. Although metallic materials show efficient adsorption performance, the specific surface area of common metal oxides is generally low, which is unfavorable for adsorption, while nano-metal oxides, although having high specific surface area, mainly suffer from the problems of difficult to completely separate and secondary contamination of residues [25].

Metal-organic skeletons (MOFs), coordination structures of organic ligands containing potential voids [26]. The arrangement of organic ligands with metal ions or clusters in MOFs has a distinct orientation, which can form different framework pore structures and exhibit excellent adsorption properties [27]. Li, J et al [28] found that MOFs, based on their highly porous and chemically stable characteristics, are able to exhibit excellent adsorbent potential for the effective removal of toxic and radioactive metal ions from the environment, especially for F ions. Ke, F et al [29] synthesized two materials, MOF-801 and CaFu-MOF, with a maximum adsorption of 32.13 mg/g of F ions in brick tea for F ion removal, showing excellent adsorption performance and selectivity. Mechanistic studies have shown that fluoride replaces the hydroxyl groups on the metal nodes in the structure of MOFs through anion exchange behavior [30]. Therefore, the pH of the solution is important for fluoride removal, which affects the surface charge of the adsorbent. Although MOFs materials have good adsorption properties and selectivity, there is still a need to overcome their poor stability at different pH values [31].

Metal composites are a kind of materials formed by metallurgically combining two or more metallic or nonmetallic materials with different chemical and mechanical properties at the interface through composite technology [32]. This kind of material not only retains the characteristics of metal materials with efficient adsorption performance, strong affinity for fluorine, and abundant surface hydroxyl groups, but also significantly improves the problems of low specific surface area, secondary contamination, and poor stability of MOFs by the addition of reinforcing materials. The Fe-La-Ce trimetallic composite prepared by Thathsara, S. K. T et al [33] achieved a maximum adsorption of fluoride ions of 303.03 mg/g at pH 4.0, which is higher than most of the reported adsorbents, and moreover combines good regeneration ability (96.13% desorption rate) and reusability, which makes it a potentially ideal fluoride removal It is a potentially ideal adsorbent for fluoride removal. Faisal, H. A et al [34] studied a cerium impregnated activated carbon (AC-Ce) metal composite and analyzed its performance for fluoride removal in fixed bed column filters. Guo, W et al [35] proposed an efficient carbon fiber-loaded Mg-Fe binary metal composite adsorbent for fluoride removal with an adsorption capacity of up to 249.0 mg/g, and analyzed the adsorption mechanism by means of a secondary kinetic model and Langmuir isotherm model calculations.

This paper starts with a quasi-primary kinetic model and a quasi-secondary kinetic model, which together form the adsorption kinetic model. The intergranular diffusion model was expressed by the formula for describing the adsorption process of materials with pores, and the Langmuir adsorption isotherm and Freundlich isotherm were applied to express the non-homogeneous adsorption system. The reagents and apparatus required for the experiment were selected, the activated alumina used for the test was pretreated, and the intermittent adsorption

test was designed. Subsequently, the micromechanical characterization of the adsorption process of activated alumina was analyzed using instruments and methods such as X-ray diffractometer, Fourier transform-infrared spectroscopy, thermogravimetric analysis, specific surface area and pore structure determination, and X-photoelectronic energy spectroscopy.

II. Experimental methods and materials

II. A. ***Adsorption kinetic modeling***

The adsorbent is added to the solution to be adsorbed, the adsorbent will be adsorbed by the adsorbent and the amount of adsorbent that can be adsorbed by the adsorbent per unit of time is known as the adsorption rate. In the process of adsorption, the reaction rate equation is the adsorption rate equation. Adsorption rate as the actual adsorption process is one of the very important parameters, the adsorption process are required to discuss it, the commonly used adsorption rate models are quasi-primary kinetic model and quasi-secondary kinetic model, etc. [36]. By fitting the adsorption rate curve data with the kinetic model, the adsorption rate curve can be judged to be more in line with which model, which in turn is conducive to the investigation of the adsorption mechanism in the adsorption process.

II. A. 1) Quasi-Level Dynamics Model

In a quasi-primary kinetic reaction, the movement of adsorbate from solution to the surface of the adsorbent is controlled by a diffusion step, and at this point there is one and only one adsorption site on the surface of the adsorbent. The expression is shown in equation (1):

$$\frac{dq_t}{dt} = k_1\left(q_{e1} - q_t\right) \tag{1}$$

Integral collation is obtained:

$$\ln\left(q_{e1} - q_t\right) = \ln q_{e1} - k_1 t \tag{2}$$

where q_{e1} is the quasi-primary kinetic equilibrium adsorption amount, mg/g, q_t is the adsorption amount at time t, mg/g, k_1 is the quasi-primary kinetic constant, min-¹, and t is the adsorption time, min.

Although quasi-primary kinetic modeling has been applied to various adsorption processes on a large scale and is well received, it has some limitations. The linear plot fitted by the quasi-primary kinetic equation is plotted by $\ln\left(q_{e1} - q_t\right)$ against time t, and therefore the value of q_{e1} has to be obtained first. However, it is possible that in the actual adsorption process, the adsorption rate is too slow, which leads to a long time to reach the equilibrium of the adsorption, and therefore the equilibrium adsorption time, min, cannot be measured very accurately. The equilibrium adsorption amount q_{e1} value is measured very accurately, therefore, the quasi-one-stage kinetic model can not describe the whole process of adsorption accurately, and it is only suitable for describing the kinetics of the initial stage of adsorption.

II. A. 2) Quasi-secondary kinetic models

The quasi-secondary kinetic modeling is based on the assumption that the adsorption rate is controlled by the chemisorption mechanism, where the adsorption process involves the sharing or transfer of electron pairs between the adsorbent and the adsorbate in solution. The presence of two binding sites on the surface of the adsorbent allows the adsorbate to reach the surface of the adsorbent under the control of the chemisorption mechanism, which is pulled by forces from the solution. Compliance with the quasi-secondary kinetic model suggests that the adsorption kinetics are mainly controlled by chemisorption and not by a physical transport step. The expression is shown in equation (3):

$$\frac{dq_t}{dt} = k_2(q_{e2} - q_t)^2 \tag{3}$$

The points are sorted out afterward:

$$\frac{t}{q_t} = \frac{1}{k_2 q_{e2}^2} + \frac{t}{q_{e2}} \tag{4}$$

where, q_{e2} is the quasi-secondary kinetic equilibrium adsorption amount, mg/g, q_t is the adsorption amount at time t, mg/g, k_2 is the quasi-secondary kinetic constant, min-¹, and t is the adsorption time, min.

II. A. 3) Interparticle diffusion model

The intergranular diffusion model is sometimes well suited to describe the adsorption process of materials with pores, and is expressed as [37]:

$$Q_t = k_i \cdot t^{\frac{1}{2}} \tag{5}$$

where: Q_t, t is the same as equation (5), $k_i\left(mg \cdot g^{-1} \cdot \min^{-\frac{1}{2}}\right)$ is the granular diffusion rate constant, and Q_t is plotted against $t^{\frac{1}{2}}$, if the curve passes through the origin of the coordinates, then the rate-limiting step of the adsorption process is inter-particle diffusion.

II. B. Adsorption isotherm model

II. B. 1) Langmuir isotherms

Langmuir isotherm describes the adsorption as a monomolecular layer with uniform distribution of individual adsorption sites on the surface of the adsorbent, but these adsorption sites are finite and the Langmuir isotherm equation is expressed as follows [38]:

$$\frac{C_e}{Q_e} = \frac{1}{b \cdot Q_m} + \frac{C_e}{Q_m} \tag{6}$$

An important property of the Langmuir adsorption isotherm can be characterized by the separation constant R_L, the magnitude of which reflects the ease or difficulty of adsorption, $R_L = 0$, indicating that the adsorption is irreversible, and $0 < R_L < 1$, indicating that the adsorption process is easy to carry out. $R_L = 1$, indicating that the adsorption isotherm is linear, and $R_L > 1$, indicating that the adsorption is difficult to carry out, the expression is as follows:

$$R_L = \frac{1}{\left(1 + bC_0\right)} \tag{7}$$

where $C_0 mg/L$ and $C_e\left(mg/L\right)$ denote the initial and equilibrium concentrations of residual fluoride ions in solution, respectively, $Q_e\left(mg/g\right)$ denotes the equilibrium adsorption capacity, $Q_m\left(mg/g\right)$ denotes the saturated adsorption capacity of the adsorbent, and $b\left(L/g\right)$ is the constant associated with the adsorption capacity. The saturated adsorption capacity, Q_m, and the value of the constant, b, are successively found based on the intercept and the slope by graphing the plot of C_e with $\frac{C_e}{Q_e}$.

II. B. 2) Freundlich isothermal equation

Freundlich isotherm is used to describe non-homogeneous phase adsorption systems, i.e., the adsorption sites on the adsorbent surface are not homogeneous, and the adsorbent can form either a monomolecular or a multimolecular adsorption layer.The Freundlich isotherm is characterized by the fact that it does not have saturated adsorption values. Its equation is expressed as:

$$\ln Q_e = \frac{1}{n} \cdot \ln C_e + \ln K_f \tag{8}$$

where: $K_f\left(L/mg\right)$ and $\frac{1}{n}$ are constants related to the adsorption capacity and adsorption strength, and $\ln Q_e$ is plotted against $\ln C_e$, and the values of $\frac{1}{n}$ and K_f can be derived based on the slope and intercept, respectively.

II. C. Reagents and instruments required for the test

II. C. 1) Reagents required for the test

The test reagents required during the test are shown in Table 1:

Table 1: Required reagents

Reagent	Molecular formula	Relative molecular mass	Reagent grade	Producer
Sodium fluoride	NaF	42.0	AR	Shanghai Gao Shen chemical co.,LTD
Sodium hydroxide	NaOH	40	AR	Beijing chemical plant
Potassium hydrogen phthalate	C8H5KO4	204.22	AR	National drug group
Hydrochloric acid	HCl	36.46	AR	Beijing chemical plant
Potassium nitrate	KNO3	101.1	AR	National drug group
Sodium chloride	NaCl	58.5	AR	Taikata meida reagent company

Activated alumina, particle size: 2~3 mm, Manufacturer: Shandong Zibo Henghuan Aluminum Co., LTD.

II. C. 2) Instruments required for the test

The main equipment and instruments used in the test are shown in Table 2:

Table 2: Required instruments

Equipment	Model number	Producer	Instrument use
Thermostatic incubator	HZQ-X100	Taig experimental equipment factory	Adsorbent performance evaluation
Analytical balance	FA2004	Tianjin tianma equipment factory	Adsorbent preparation
Microcomputer type desktop PH meter	PHS-3C	Shanghai kang yi instrument co., LTD	Absorptivity can be evaluated
Standard screen	-	Zhejiang yongkang golden ear machinery factory	Adsorbent preparation
Digital constant magnetic stirrer	85-2	Shanghai syle instrument co., LTD	Adsorbent preparation
Full automatic potentiometric titrator	ZDJ-2D+	Beijing pioneer weifeng technology development company	PH buffer and absorpability can be evaluated
High speed multi-function mill	JSP-100	Golden ear instrument factory	Adsorbent preparation
Conductivity meter	DS-11A	Shanghai bewei technology co., LTD	Absorptivity can be evaluated
Electric thermostat	DH-101D	Beijing likang da SAN technology co., LTD	Preparation/performance of adsorbent
Fluorine ion selection electrode	PF-1	Shanghai kang yi instrument co., LTD	Absorptivity can be evaluated
Centrifuge	TDL-40B	Wuxi ruijiang analyzer co., LTD	Absorptivity can be evaluated

II. D.Test methods

II. D. 1) Pretreatment with activated alumina

The activated alumina GAA powder used in the experiment was crushed from GAA particles, and the crushed GAA powder was poured into a standard sieve for sieving, and the particle size of activated alumina powder was selected as 80-150 mesh for this experiment, and the sealing equipment was used [39].

II. D. 2) Intermittent adsorption tests

The intermittent adsorption test includes two parts, the intermittent isothermal experiment as well as the kinetic experiment, and the specific experimental flow is shown in Fig. 1, which can be referred to in other sections of this paper.

Figure 1: Process flow for adsorption experiment

(1) Adsorption isothermal test

1) Take 12 150mL conical flasks, add 100ml of fluorine solution with different initial concentrations, and add a certain amount of HCI solution to adjust the initial pH of the solution to 5.0±0.2.

2) Similarly, 12 portions of GAA were accurately weighed, each portion (100±3) mg, were put into the above 12 conical flasks, which were placed in a thermostatic oscillator to carry out adsorption by oscillation for 12h, with the temperature set at 25℃ and the rotational speed adjusted to 180r/min.

3) After 12h of adsorption, the suspension was fully centrifuged and filtered by adding 0.45um microporous filter membrane, and the residual F concentration in the filtrate was determined according to the fluoride ion-selective electrode method and the adsorption amount was calculated.

(2) Adsorption kinetic test

1) Add 100 ml of fluorine-containing water samples with initial F concentrations of 5.0 and 20.0 mg/L into a conical flask, and add a small amount of HCl solution to adjust the initial pH of the solution to 5.0±0.2.

2) Accurately weigh the GAA powder (100±3) mg into the above conical flask, placed in a pre-set speed of 180 r/min, temperature 25 ℃ constant temperature oscillator oscillation.

3) Take out the above suspension at regular intervals, centrifuge it in a centrifuge with the rotational speed set at 4000 r/min, filter it with 0.45 um microporous filter membrane after sufficient centrifugation, and then determine the residual F concentration in the filtrate according to the fluoride ion-selective electrode method and calculate the adsorption amount.

II. E. Methods for characterization and analysis of micro-mechanisms of materials

II. E. 1) X-ray diffraction analysis (XRD)

An X-ray diffractometer (Model: TTRIII) was utilized to determine the phase composition of the samples. The scanning range20 was from 5° to 60° with voltage and current of 40 KV and 250 mA, respectively, and scanning speed of 9/min, 0.02°/step, DS=SS=1°, RS-0.15 mm [40].

II. E. 2) Fourier Transform Infrared Spectroscopy (FTIR)

The synthesized samples were measured by using Thermo's FT-IR instrument (model: Thermo Nicolet) to analyze the functional groups on the surface of the samples at a wavelength of 400-4000 cm〃1. Sample preparation: The samples were ground and mixed with KBr in the ratio of about 1:100, and then finally pressed into transparent flakes.

II. E. 3) Thermogravimetric analysis (TG/TGA)

The thermal stability and weight loss of the synthesized samples were determined by using a METTLER thermogravimetric analyzer (Model: METTLER HT/1600) with a heating rate of 5 °C/min and a temperature range of 20 °C to 900 °C. The samples were analyzed by using a thermogravimetric analyzer (Model: METTLER HT/1600).

II. E. 4) Determination of specific surface area and pore structure

The specific surface area, pore volume and pore size of the adsorbents were determined using an N_2 adsorption specific surface area tester (model: TriStar 11 3020) from Micromeritics, USA. Among them, the specific surface area of the material (SBET) was obtained according to the BET and Langumuir methods, the pore volume and pore size of the material were calculated using the BJH method, and the pore size distribution was determined by the density flooding method (DFT).

II. E. 5) X-photoelectron spectroscopy (XPS)

The surface composition of the synthesized samples and products was determined using a ULVAC-PHI Inc XPS (model: PHI5000X). The radiation source was Ka-rays of monochromatic Al, corrected with Cls of 284.8 eV.

III. Calculation of the dynamics and micromechanism of fluoride ions on the surface of metallic composites

III. A. Kinetics of Fluoride Ion Adsorption Processes on Metal Composite Surfaces

III. A. 1) Adsorption kinetics analysis

Fig. 2 shows the proposed primary and proposed secondary kinetic models of activated alumina (GAA). In this case, Fig. (a) shows the proposed primary and Fig. (b) shows the proposed secondary kinetic model of activated alumina (GAA). The fit R^2 of the proposed secondary kinetics at reagent concentrations of 10 mg/L, 30 mg/L, and 100 mg/L were all 0.9999, and the fit of the proposed secondary kinetic model was much higher than that of the proposed primary kinetic model, and the value of q_e obtained from the proposed secondary kinetic model was much closer to the actual value, so that the proposed secondary kinetic model was more in line with the adsorption process of activated alumina (GAA).) adsorption process.

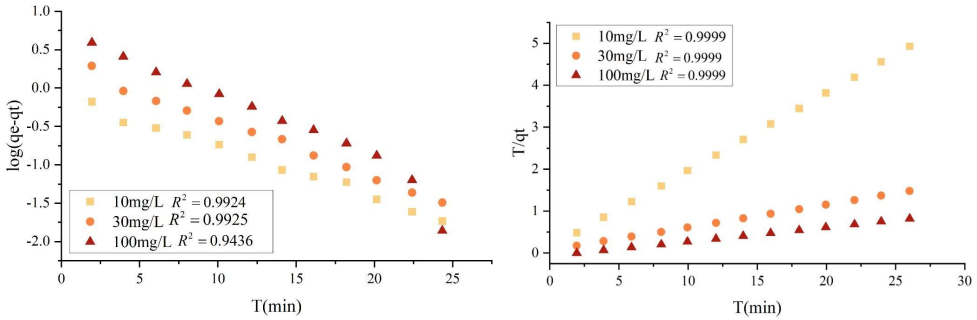

(a)The quasi primary kinetic model of active oxygen aluminum (GAA)

(b)The quasi-secondary dynamics model of activated aluminum (GAA)

Figure 2: Pseudo-first-order and pseudo-second-order kinetics parameters

III. A. 2) Intra-particle diffusion kinetics

In addition, the intra-particle diffusion kinetic model allows the adsorption of fluorine to be divided into three stages, which are controlled by different diffusion mechanisms. Figure 3 shows the intra-particle diffusion type fitting curve and Table 3 shows the parameters of the intra-particle diffusion kinetic model fitting. The highest rate of k_i was observed in the first stage, when thin-film diffusion was the main form of diffusion, which was accomplished within the first 10 min at rates of 6.1356, 11.2485, and 17.2456, respectively.In the second stage, the fluorine adsorption on the adsorbent occurred gradually at a relatively slow rate, followed by the saturation of adsorption in the third stage. It is noteworthy that the fitted curves for each stage have intercepts, indicating that the adsorption process of activated alumina (GAA) on fluoride is not only affected by ionic diffusion, but also by external mass transfer, surface adsorption and pore diffusion.

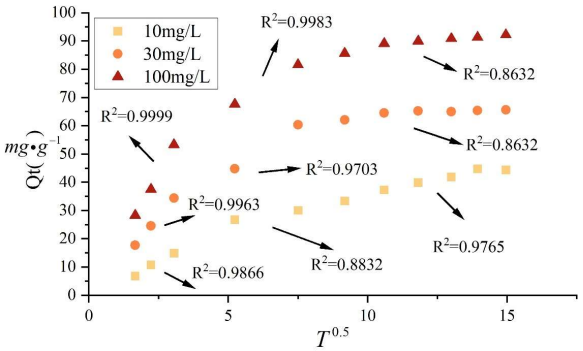

Figure 3: Intergranular dispersion curve

Table 3: Particle diffusion dynamics model parameters

Adsorbents	Step1		
	$k_i(mg·g^{-1}/\min^{0.5})$	$C(mg·g^{-1})$	R^2
10mg/L	6.1356	-4.4368	0.9866
30mg/L	11.2485	-1.9478	0.8832
100mg/L	17.2456	-2.0965	0.9765
	Step2		
10mg/L	3.2644	5.8456	0.9963
30mg/L	5.7453	14.6234	0.9703
100mg/L	6.1306	33.4648	0.8632
	Step3		
10mg/L	1.9455	14.9315	0.9999
30mg/L	0.6634	55.3136	0.9983
100mg/L	1.4645	71.3972	0.8632

III. B. ***Analysis of adsorption isotherm fitting results***

Adsorption isotherm is the thermodynamic data obtained by analyzing the relationship between the concentration of adsorbent in solution and the concentration of adsorbent on the adsorbent at the adsorption equilibrium at a certain temperature. When the temperature or concentration is fixed, the equilibrium adsorption capacity during the adsorption reaction is a single-valued function of concentration or temperature. The adsorption equilibrium data were analyzed by the classical Langmuir, Freundlich, and Temkin adsorption isotherm equations, and the results are shown in Fig. 4, the adsorption of F- by activated alumina (GAA) is more consistent with the Freundlich model. It can be concluded that the active sites on the adsorbent would interact with each other and thus between the F- adsorbed to it, and at the same time inhibit the further adsorption of free state F- on the adsorbent, so the theoretically calculated adsorption capacity is usually much larger than the actual adsorption amount. In addition, it is worth mentioning that the Temkin adsorption isotherm also fits the data relatively well, and its correlation coefficient R^2 value reaches 0.9453.This indicates that the heat of adsorption decreases with increasing adsorption capacity during the adsorption of F-.The conformity of both Freundlich adsorption and Temkin adsorption suggests that the process of activated alumina (GAA) in the adsorption of F- is an process with changing enthalpy change.

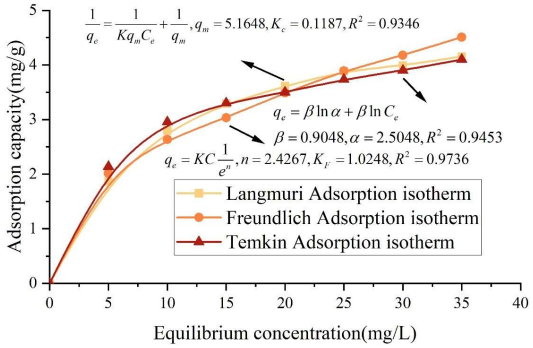

Figure 4: Results of adsorption isotherm fitting

Note : q_m indicates the maximum adsorption capacity of the adsorbent (mg/g), q_e represents the F-concentration on the adsorbent at equilibrium (mg/g), n is a constant that changes with the change of adsorbent and adsorbed ion, and Daqian 1, KC, K_F, α, β represent constants related to adsorption temperature, adsorption system, etc.

III. C. Mechanism of microscopic characterization of the adsorption process of metal-conforming materials

III. C. 1) XRD

For the physical phase and crystalline structure of activated alumina (GAA) loaded on the surface of the composites, the activated alumina (GAA) was analyzed by X-ray diffraction (XRD), and the results are shown in Fig. 5.The diffraction peaks at 25° were generated by the Al3+ (005) crystal facets indicating the presence of aluminum ions, and the diffraction peaks at 30.2°, 35.3°, 50.2° and 60.2° were produced by the (010), (123), (115) and (133) crystal faces of tetragonal phase activated alumina (GAA), and the characteristic peaks appearing at 28°, 31.2° are the (-124) and (124) crystal faces of monoclinic phase activated alumina (GAA), and these results indicate that the aluminum alloy in the activated alumina (GAA) is characterized by a mixture of the tetragonal and monoclinic phases.

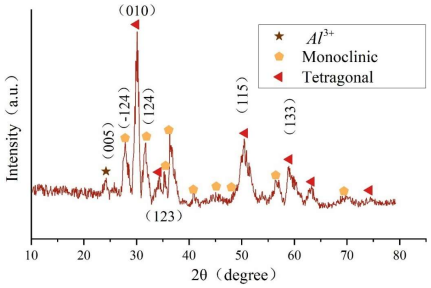

Figure 5: XRD patterns of GAA

III. C. 2) FTIR

In order to analyze the functional groups of activated alumina (GAA) and their effects on the adsorption of fluoride ions, the activated alumina (GAA) was characterized before and after the adsorption using Fourier infrared spectroscopy, and the results are shown in Fig. 6. The absorption peak appearing around 3323 cm^{-1} is the O-H stretching vibration absorption peak, and at 2936 cm^{-1} is the C-H stretching vibration, which corresponds to the C=0 bond at the peak value of 1689 cm^{-1}. The absorption peak in the region of 1226-1400 cm^{-1} attributed to the stretching vibration of the benzene ring skeleton is at 553 cm^{-1}, and the peak appearing is Fe-O. The range and intensity of the peaks on the surface of activated alumina (GAA) after adsorption of fluoride ions change significantly, which may be due to the interaction between the functional group and fluorine.

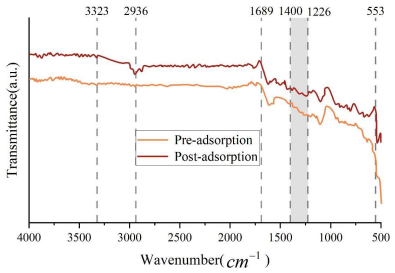

Figure 6: FT-IR spectrum of GAA before and after adsorption

III. C. 3) Thermogravimetric analysis

Specific surface area and porosity thermogravimetric analysis of alumina and activated alumina were further analyzed using N2 adsorption-desorption isotherms and are shown in Fig. 7, with adsorption-desorption isotherms thermogravimetrically in Fig. (a) and pore size distribution thermogravimetrically in Fig. (b). Alumina and activated alumina show typical type IV isotherms of the isotherm types suggested by IUPAC (International Union of Pure and Applied Chemistry), which indicates the presence of mesopores in the materials. The pore sizes of alumina and activated alumina were 7.5644 nm and 26.9946 nm, respectively, which were larger than the diameter of fluoride ions, suggesting that fluoride ions not only diffuse to the surface of the mesoporous materials of the metal composites, but also penetrate into the pores and further bind to the adsorption sites within the adsorbent. Notably, the BET specific surface area of activated alumina is significantly larger than that of alumina crystals, with the specific surface area of activated alumina approaching 27 cm^3g^{-1}, which is larger than that of alumina, which is 6 cm^3g^{-1}, implying that activated alumina synthesized in the adjusted solvent would increase the exposure of active sites.

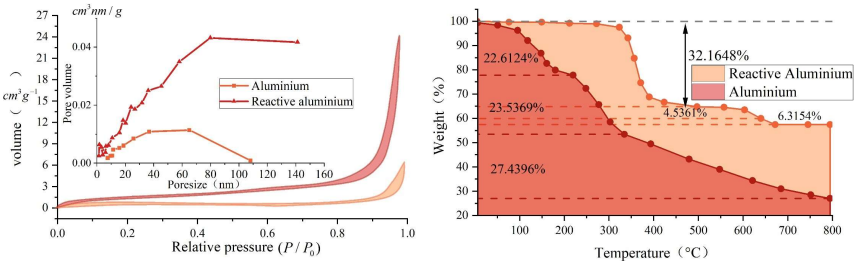

(a)Adsorption - the heat of the isotherm (b)Aperture distribution heat weight

Figure 7: Thermal reanalysis

The thermogravimetric diagram presented in Figure (b) shows that the synthesized activated alumina has better thermal stability than alumina. The mass of alumina starts to decrease rapidly between 100-248°C due to the volatilization of the micro hydrated DMF mixture in the structure of the material, the rapid decrease may be due to the inclusion of more water and DMF mixture. The second phase of rapid decrease occurs between 248-350 °C, the mass decreases sharply from 78% to 54%, probably due to the conversion of organic ligands to carbonates.The mass starts to decrease slowly after 400 °C, which is the generation of alumina, and by 800 °C the residual mass is left at 26.4111%. Activated alumina is relatively better thermally stable, with almost no change in mass until 356 °C, and only after 356 °C does it begin the first period of rapid mass decrease, and at 800 °C, the residual mass is still 56.9837% left, which indicates that activated alumina is a strong metallic structure with high

thermal stability, and that activated alumina synthesized in one step of hydrothermal synthesis is thermally stable, good structural properties prompted further exploration of the adsorption properties of the material.

III. C. 4) Specific surface area and pore size analysis

The specific surface area of the adsorbent is an important factor affecting the adsorption efficacy. Based on the adsorption-desorption curves and data of the material under N2 conditions measured by the fully automatic specific surface area analyzer, the parameters of the material such as specific surface area, pore volume and pore size distribution were calculated.

In the following, the specific surface area and pore size analysis of tetragonal phase activated alumina. The results of adsorption-desorption curves and total pore size distribution of tetragonal phase iron oxides are shown in Fig. 8, Figs. (a)-(c) show the adsorption (ADS) and desorption (DES) curves of alumina {010}, activated alumina {010}, and activated alumina {115}{133}, and Figs. (d)-(f) show the adsorption and desorption curves of alumina {010}, activated alumina {010}, and activated alumina {115}{133} of total pore size distribution. According to the pore size distributions, all the three prepared tetragonal phase iron oxides are mesoporous materials, and the hysteresis loops are type IV hysteresis loops, reflecting the mesoporous properties. The pore size distribution of alumina {010} is mainly in the regions of 30-55 nm as well as 73-86 nm, with a small number of micropores as well as mesopores. The pore size distribution of alumina {010} and activated alumina {115}{133} is mainly in the region of 25~55 nm, with a certain proportion of micropores.

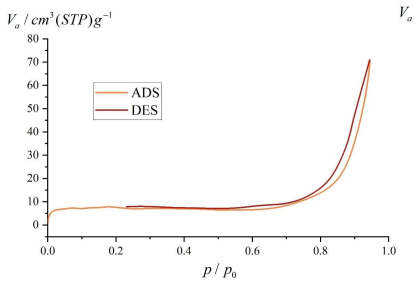

(a)Aluminium oxide {010} ADS and DES

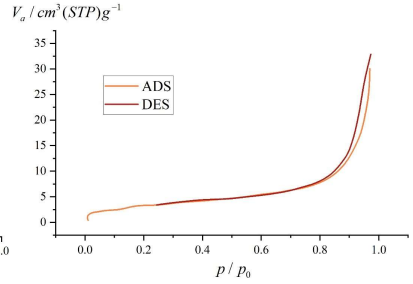

(b)Reactive aluminium oxide {010} ADS and DES

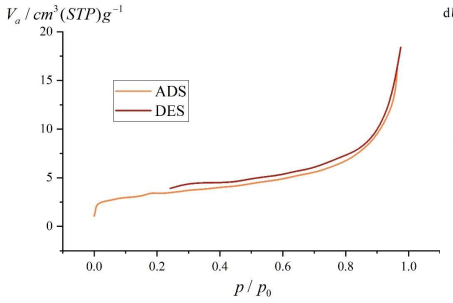

(c)Reactive aluminium oxide {115}{133} ADS and DES

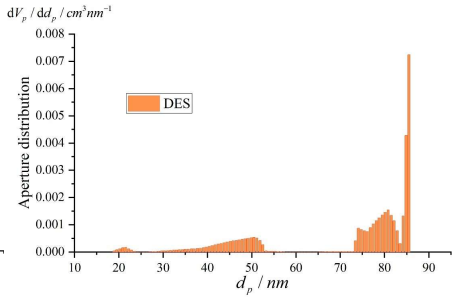

(d)Aperture distribution of Aluminium oxide {010}

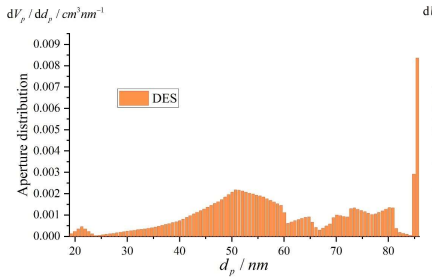

(e)Aperture distribution of Reactive aluminium oxide {010}

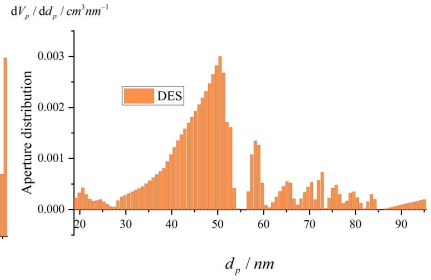

(f)Aperture distribution of Reactive aluminium oxide {115}{133}

Figure 8: The adsorption of the quadrangle GAA and the total aperture distribution

III. C. 5) X-photoelectron spectroscopy

XPS analysis provided further support for the mechanism of fluoride adsorption on the absorbent. The full XPS spectrum of activated alumina (GAA) is shown in Fig. 9.The full XPS spectrum of activated alumina (GAA) shows the presence of Al, O, and C. After adsorption, a new peak at 702.4553 eV was observed for activated alumina (GAA) C, which corresponds to the F1s, indicating that the fluoride species was successfully loaded on the activated alumina (GAA) adsorbent. The intensity of the Al-OH peak was reduced due to the binding of Al with fluoride.

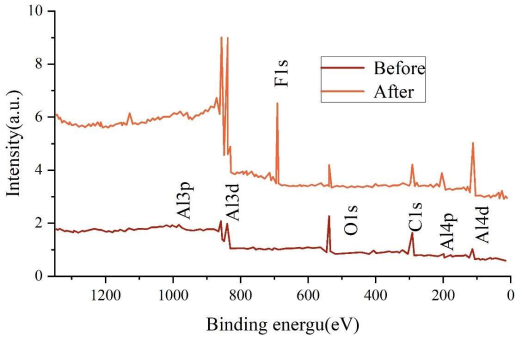

Figure 9: XPS spectrum

IV. Conclusion

In this paper, the adsorption kinetic model and adsorption isotherm model were constructed at the same time, the reagents and instruments required for the experiment were selected, and the interstitial adsorption test was designed. The kinetic and microscopic mechanisms of the adsorption process on the surface of metal composites were investigated by XRD, FTIR and XPS.

(1) The fitted secondary kinetics had a fit R^2 of 0.9999 at reagent concentrations of 10 mg/L, 30 mg/L, and 100 mg/L, respectively.In the intra-particle diffusion kinetic model, the adsorption of fluorine was divided into three phases, and the highest diffusion rate was observed in phase 1, with rates of 6.1356, 11.2485, and 17.2456, respectively, and the diffusion was completed within the first 10 minutes.

(2) The adsorption of F- by activated alumina (GAA) was more in line with the Freundlich model, with a goodness of fit R^2=0.9736, which was the best performance among the three adsorption isotherm equations, indicating that the adsorption process of activated alumina (GAA) in the adsorption process of F- is a process of constant change in enthalpy.

(3) The functional groups of activated alumina (GAA) and their effects on the adsorption of fluoride ions were analyzed using Fourier infrared spectroscopy. The absorption peaks appearing around 3323 cm^{-1} are the O-H stretching vibration absorption peaks, and the C-H stretching vibration at 2936 cm^{-1}, and at the peak value of 1689 cm^{-1} at which corresponds to C=0 bond. Meanwhile, XPS was used to further analyze the adsorption mechanism of fluoride on the sorbent, and after adsorption, a new peak of activated alumina (GAA) C was observed at 702.4553 eV, which corresponds to F1s, indicating that the fluoride species was successfully loaded on the activated alumina (GAA) sorbent.

References

[1] Ali, S., Thakur, S. K., Sarkar, A., & Shekhar, S. (2016). Worldwide contamination of water by fluoride. Environmental chemistry letters, 14, 291-315.

[2] Peckham, S., & Awofeso, N. (2014). Water fluoridation: a critical review of the physiological effects of ingested fluoride as a public health intervention. The Scientific World Journal, 2014(1), 293019.

[3] Kabir, H., Gupta, A. K., & Tripathy, S. (2020). Fluoride and human health: Systematic appraisal of sources, exposures, metabolism, and toxicity. Critical Reviews in Environmental Science and Technology, 50(11), 1116-1193.

[4] Lubojanski, A., Piesiak-Panczyszyn, D., Zakrzewski, W., Dobrzynski, W., Szymonowicz, M., Rybak, Z., ... & Dobrzynski, M. (2023). The safety of fluoride compounds and their effect on the human body—A narrative review. Materials, 16(3), 1242.

[5] Dharmaratne, R. W. (2019). Exploring the role of excess fluoride in chronic kidney disease: a review. Human & experimental toxicology, 38(3), 269-279.

[6] Singh, J., Singh, P., & Singh, A. (2016). Fluoride ions vs removal technologies: A study. Arabian Journal of Chemistry, 9(6), 815-824.

[7] Fu, F., & Wang, Q. (2011). Removal of heavy metal ions from wastewaters: a review. Journal of environmental management, 92(3), 407-418.

[8] Bhatnagar, A., Kumar, E., & Sillanpää, M. (2011). Fluoride removal from water by adsorption—a review. Chemical engineering journal, 171(3), 811-840.

[9] Chen, N., Zhang, Z., Feng, C., Sugiura, N., Li, M., & Chen, R. (2010). Fluoride removal from water by granular ceramic adsorption. Journal of colloid and interface science, 348(2), 579-584.
[10] Ramdani, A., Taleb, S., Benghalem, A., & Ghaffour, N. (2010). Removal of excess fluoride ions from Saharan brackish water by adsorption on natural materials. Desalination, 250(1), 408-413.
[11] John, Y., David Jr, V. E., & Mmereki, D. (2018). A comparative study on removal of hazardous anions from water by adsorption: a review. International Journal of Chemical Engineering, 2018(1), 3975948.
[12] Ashiq, A., Vithanage, M., Sarkar, B., Kumar, M., Bhatnagar, A., Khan, E., ... & Ok, Y. S. (2021). Carbon-based adsorbents for fluoroquinolone removal from water and wastewater: a critical review. Environmental Research, 197, 111091.
[13] Biswas, G., Kumari, M., Adhikari, K., & Dutta, S. (2017). A critical review on occurrence of fluoride and its removal through adsorption with an emphasis on natural minerals. Current Pollution Reports, 3, 104-119.
[14] Seruga, P., Krzywonos, M., Pyżanowska, J., Urbanowska, A., Pawlak-Kruczek, H., & Niedźwiecki, Ł. (2019). Removal of ammonia from the municipal waste treatment effluents using natural minerals. Molecules, 24(20), 3633.
[15] Ben Amor, T., Kassem, M., Hajjaji, W., Jamoussi, F., Ben Amor, M., & Hafiane, A. (2018). Study of defluoridation of water using natural clay minerals. Clays and Clay Minerals, 66, 493-499.
[16] Yi, M., Wang, K., Wei, H., Wei, D., Wei, X., Wei, B., ... & Cui, X. (2023). Efficient preparation of red mud-based geopolymer microspheres (RM@ GMs) and adsorption of fluoride ions in wastewater. Journal of Hazardous Materials, 442, 130027.
[17] Phillips, D. H., Gupta, B. S., Mukhopadhyay, S., & Gupta, A. K. S. (2018). Arsenic and fluoride removal from contaminated drinking water with Haix-Fe-Zr and Haix-Zr resin beads. Journal of Environmental Management, 215, 132-142.
[18] Gao, Y., Deng, S., Du, Z., Liu, K., & Yu, G. (2017). Adsorptive removal of emerging polyfluoroalky substances F-53B and PFOS by anion-exchange resin: A comparative study. Journal of Hazardous Materials, 323, 550-557.
[19] Alrowais, R., Bashir, M. T., Sikandar, M. A., & Khan, M. A. (2022). Synthesis and performance evaluation of olive fruit waste resin for removal of fluoride from aqueous solution: batch and column modeling. Desalination and Water Treatment, 252, 261-275.
[20] Pašti, I. A., Gavrilov, N. M., & Mentus, S. V. (2013). Fluorine adsorption on transition metal surfaces: A DFT study. Journal of the Serbian Chemical Society, 78(11), 1763-1773.
[21] Gasparotto, J. M., Roth, D., Perilli, A. L. D. O., Franco, D. S., Carissimi, E., Foletto, E. L., ... & Dotto, G. L. (2021). A novel Fe-Al-La trioxide composite: Synthesis, characterization, and application for fluoride ions removal from the water supply. Journal of Environmental Chemical Engineering, 9(6), 106350.
[22] Zhou, Q., Ren, B., Wei, Y., Tian, S., Jin, X., Jiang, F., ... & Yang, X. (2025). Efficient removal of fluoride from water: Adsorption performance of MgO-x adsorbents derived from Mg-MOF-74 and insights from DFT calculations. Separation and Purification Technology, 352, 128190.
[23] Yang, K., Li, H., Lin, W., Chen, Z., Peng, S., Yu, K., & Fang, Z. (2024). Performance and mechanism of hierarchical porous Al2O3-MgO nanosheets for removing fluoride ions from industrial ZnSO4 solution. Separation and Purification Technology, 330, 125255.
[24] Guo, W., Lin, H., Zhu, H., Lei, M., & Feng, J. (2023). Preparation and application of magnesium oxide nanoparticles for superiorly fluoride removal. Journal of Alloys and Compounds, 960, 170935.
[25] Sylwan, I., & Thorin, E. (2021). Removal of heavy metals during primary treatment of municipal wastewater and possibilities of enhanced removal: A review. Water, 13(08), 1121.
[26] Kitagawa, S. (2014). Metal–organic frameworks (MOFs). Chemical Society Reviews, 43(16), 5415-5418.
[27] Zhu, X. H., Yang, C. X., & Yan, X. P. (2018). Metal-organic framework-801 for efficient removal of fluoride from water. Microporous and Mesoporous Materials, 259, 163-170.
[28] Li, J., Wang, X., Zhao, G., Chen, C., Chai, Z., Alsaedi, A., ... & Wang, X. (2018). Metal–organic framework-based materials: superior adsorbents for the capture of toxic and radioactive metal ions. Chemical Society Reviews, 47(7), 2322-2356.
[29] Ke, F., Peng, C., Zhang, T., Zhang, M., Zhou, C., Cai, H., ... & Wan, X. (2018). Fumarate-based metal-organic frameworks as a new platform for highly selective removal of fluoride from brick tea. Scientific reports, 8(1), 939.
[30] Chen, Y., Bai, X., & Ye, Z. (2020). Recent progress in heavy metal ion decontamination based on metal–organic frameworks. Nanomaterials, 10(8), 1481.
[31] Xu, G. R., An, Z. H., Xu, K., Liu, Q., Das, R., & Zhao, H. L. (2021). Metal organic framework (MOF)-based micro/nanoscaled materials for heavy metal ions removal: The cutting-edge study on designs, synthesis, and applications. Coordination Chemistry Reviews, 427, 213554.
[32] Alhassan, S. I., Huang, L., He, Y., Yan, L., Wu, B., & Wang, H. (2021). Fluoride removal from water using alumina and aluminum-based composites: A comprehensive review of progress. Critical Reviews in Environmental Science and Technology, 51(18), 2051-2085.
[33] Thathsara, S. K. T., Cooray, P. L. A. T., Mudiyanselage, T. K., Kottegoda, N., & Ratnaweera, D. R. (2018). A novel Fe-La-Ce tri-metallic composite for the removal of fluoride ions from aqueous media. Journal of Environmental Management, 207, 387-395.
[34] Faisal, H. A., Kar, A., & Raychoudhury, T. (2019). Fluoride removal by novel composite material and its performance in the fixed-bed column filter. Current Science, 116(12), 2077-2083.
[35] Guo, W., Lin, H., Zhu, H., Mo, W., Su, X., Yang, J., ... & Lei, M. (2024). Efficient removal of fluorine by carbon fiber supported Mg-Fe binary metal oxide composite adsorbent and mechanism analysis based on DFT. Separation and Purification Technology, 330, 125320.
[36] Mengle Huang,Chunhui Zhang,Fuqing Hou,Yadong Sun & Yifan Zhan. (2025). Optimizing surface adsorption dynamics of aramid fibers using a surfactant adsorption-diffusion kinetic model. Journal of Environmental Chemical Engineering,13(1),115056-115056.
[37] Mishra Pratyush,Yavas Denizhan,Alshehri Abdullah,Shrotriya Pranav,Bastawros Ashraf & Hebert Kurt R. (2021). Model of vacancy diffusion-assisted intergranular corrosion in low-alloy steel. Acta Materialia,220,
[38] Minh H. Dang,Nam T.P. Le & Thoai N. Tran. (2020). Second-order slip condition considering Langmuir isothermal adsorption for rarefied gas microflows. Progress in Computational Fluid Dynamics An International Journal,20(4),201.
[39] Camus Élise,Pellarin Michel,Blanchard Nicholas,Boisron Olivier,Hillenkamp Matthias,Roiban Lucian... & Cottancin Emmanuel. (2022). Structural and optical characterization of nanoalloys mixing gold or silver with aluminium or indium: evolution under various reactive environments. Faraday discussions,242,
[40] Hernán D. Sánchez,Eduardo L. Gutiérrez,Marcos G. Russo,Florencia Di Salvo,Carlos R. Pungitore & Hugo A. Garro. (2025). Determining the crystal structure and the absolute configurations of decompostin from Senecio Subulatus by X-ray diffraction studies and NMR spectroscopy. Journal of Molecular Structure,1332,141681-141681.